ADVANCED QUANTUM TECHNOLOGIES
www.advquantumtech.com

Quantum Artificial Synapses

*You Meng, Sen Po Yip, Wei Wang, Chuntai Liu, and Johnny C. Ho**

Neuromorphic in-memory computing systems, comprising artificial synapses and neurons, can overcome the energy inefficiency and throughput limitation of today's von Neumann computing architecture. Recently, powered by the unique properties of quantum materials, for example, high mobility, outstanding sensitivity, and strong quantum effect, researchers have built quantum artificial synapses to mimic the biological ones. These quantum electronic/photonic synapses can precisely define their conductance state (or synaptic weight) for emulating synaptic behaviors, which shows bionic performance unreachable by other conventional materials. In this review, the significant achievements in quantum artificial synapses are summarized. First, potential quantum materials used in artificial synapses are discussed with particular attention to quantum dots, nanowires, layered materials, and quasi-2DEG interfaces. Then, the major quantum effects that are utilized in quantum artificial synapses, for example, Josephson effect, quantum tunneling, and spin memory, are reviewed. In addition to the discussion on a single synaptic device, the macroscale integration into artificial visual systems and artificial nerve networks are also highlighted. Finally, the associated future research trends and target applications are also discussed.

1. Introduction

Human brain is an enormously parallel and reconfigurable neural network, which consists of $\approx 10^{11}$ neurons and $\approx 10^{15}$ synapses. Synapses are junctions among neurons, which could be enhanced or inhibited in response to spike events. Such event-dependent synaptic plasticity forms the basis of parallel computing and distributed memory.[1] Inspired by the human brain, artificial neuromorphic systems that adopt an in-memory computing approach are then developed to tackle the intrinsic energy and throughput restrictions of the typical von Neumann computing architecture.[2,3] To realize the artificial version of synapses, various synaptic device concepts were explored to resemble the ion flux and neurotransmitter release dynamics in biological synapses. Particularly, taking advantages from the dynamic changes in the synaptic connection strength, artificial synapses can efficiently manipulate data and identify patterns in a more robust, plastic and fault-tolerant manner, giving rise to the adaptivity to indeterministic information.[4–6] All these outstanding characteristics of neuromorphic computing architecture have made it of great interest for brain-inspired technological applications such as visual information processing and others.

Although significant achievements of software or hardware implementations of artificial synaptic devices and systems have been witnessed, most of their energy efficiencies are still many orders of magnitude lower than the biological ones.[7,8] Recently, low-dimensional quantum materials have emerged as leading candidate materials for the neuromorphic computing and bioelectric interface.[9–11] In contrast to the conventional materials that have been utilized in many neuromorphic devices and systems, low-dimensional quantum materials exhibit novel device functionality, better mimicking the biological neurons.[12] The rich structural and compositional manipulation of quantum materials, coupled with defect engineering and interfacial chemistry, offers significant opportunities to realize ultralow-power artificial neural networks.[9,13,14] Importantly, the diverse quantum phenomena, including carrier confinement effect, quantum tunneling effect, quantum phase transition, Josephson effect, and atomic-level control, would enable new device concepts for reconfigurable switches and also neuromorphic functions.

In this review, recent progress on the emerging quantum materials-based neuromorphic electronics are summarized. Zero-dimensional (0D) materials, involving semiconductor quantum dots (QDs), metal QDs, and core-shell QDs, exhibit the size-dependent multi-level resistive switching memory, enabled by carrier trapping and electrochemical metallization. 1D materials, represented by carbon nanotubes (CNTs) and group III-V nanowires (NWs), demonstrated multi-level resistive switching memory on the basis of surface functionalization and redox chemistry. 2D materials, such as graphene, graphene oxide, and monolayer transition metal dichalcogenides (TMDCs), provide an open platform for multiple terminal gating, in situ

Y. Meng, W. Wang, J. C. Ho
Department of Materials Science and Engineering, State Key Laboratory of Terahertz and Millimeter Waves, and Centre for Functional Photonics
City University of Hong Kong
Kowloon, Hong Kong SAR 999077, China
E-mail: johnnyho@cityu.edu.hk

S. P. Yip, J. C. Ho
Institute for Materials Chemistry and Engineering
Kyushu University
Fukuoka 816-8580, Japan

C. Liu
Key Laboratory of Advanced Materials Processing & Mold (Zhengzhou University)
Ministry of Education
Zhengzhou 450002, China

The ORCID identification number(s) for the author(s) of this article can be found under https://doi.org/10.1002/qute.202100072

DOI: 10.1002/qute.202100072

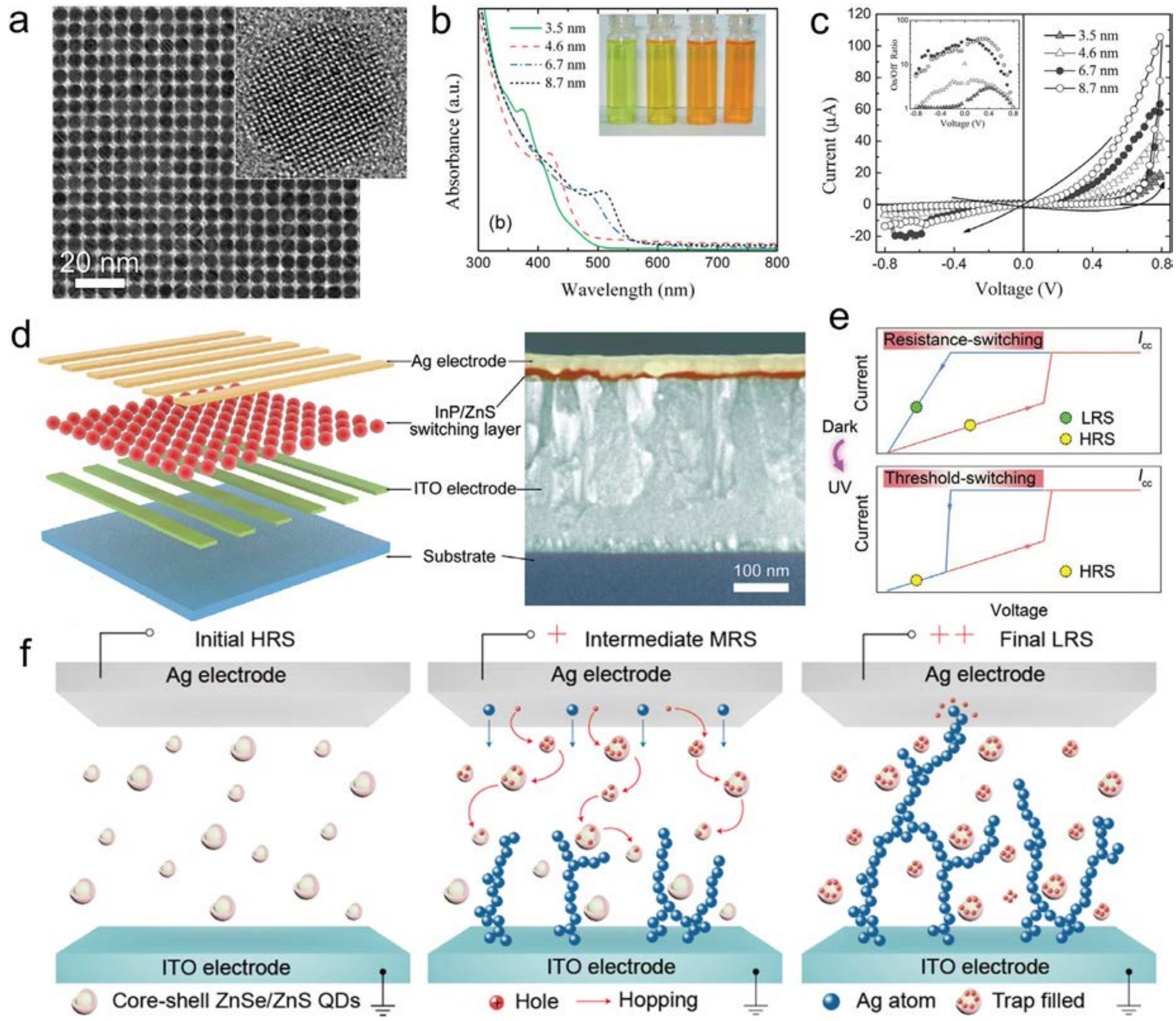

Figure 1. 0D quantum materials for artificial synapses. a) Typical TEM image and HRTEM image (inset) of PbS QDs. Reproduced with permission.[15] Copyright 2014, American Chemical Society. b) Optical absorption spectra of CdSe nanoparticles with different sizes with the inset showing the corresponding photograph in dispersed solution. c) Size-dependent electrical bistability of CdSe QDs. Reproduced with permission.[16] Copyright 2007, Wiley-VCH. d) Device architecture of core–shell InP/ZnS QDs film memristors. e) Nonvolatile resistance-switching memory (top) and volatile threshold-switching memory (bottom) of InP/ZnS QDs film memristors. Reproduced with permission.[17] Copyright 2020, Wiley-VCH. f) Multi-level resistive switching memory core–shell ZnSe/ZnS QDs with the synergistic effect between charge carrier trapping and conductive filament formation. Reproduced with permission.[18] Copyright 2020, American Chemical Society.

characterizations, and spatiotemporal synaptic responses. The quantum materials with different dimensionalities are also integrated into hybrid systems, showing promising results. In addition to summarize the above-mentioned quantum materials, various associated quantum effects are also reviewed to enable the unique neuromorphic responses, in particular Josephson effect, quantum tunneling effect, spin effect, and quantum filamentary conductance.

2. Quantum Materials for Artificial Synapses

2.1. 0D Quantum Materials for Artificial Synapses

QDs are the nanoscale crystal forms of analogous bulk crystals, which normally have diameters ranging between 2 and 20 nm (**Figure 1**a).[15] QDs offer a powerful platform to be tailored in size, shape, surface ligand, and chemical composition. Also, the associated strong quantum and dielectric confinement effects bring about the highly tunable electronic and optical properties of QDs, which in turn enriches the functions of 0D materials-based neuromorphic systems (Figure 1b).[15,19]

Metal chalcogenides QDs, which generally comprise the earth-abundant elements, is a kind of attractive low-cost materials for high-performance electronics,[20–22] near-infrared optoelectronics,[23–25] and resistive switching memory. In a pioneer study, CdSe QDs were experimentally demonstrated with the size-dependent electrical bistability and reversible memory phenomenon (Figure 1b,c),[16] highlighting that the metal chalcogenides QDs and other kind QDs would potentially serve as memory elements. In a recent work reported by Yan et al., lead sulfide (PbS) QDs with a diameter of approximately 4 nm were self-assembled into ordered networks for resistive switching, which exhibited the significantly enhanced uniformity of switching parameters, for example, the smaller threshold voltage and the narrower distribution of SET/RESET voltages.[26]

Besides, core–shell InP/ZnS QDs thin film memristors with optically modulated threshold switching were as well constructed to emulate the visual neuronal behaviors (Figure 1d).[17] The type-II energy band alignment was proposed in such InP/ZnS QDs, leading to the efficiently separation of photo-generated electron/hole pairs and thus the demonstration of light-induced threshold switching memory (Figure 1e).[17] By the same research group, core-shell ZnSe/ZnS QDs with type-I energy-band alignment were also employed to realize resistive switching.[18] With the synergistic effect between carrier trapping and electrochemical metallization, multi-level resistive switching memory with unique bipolar characteristics were demonstrated on core-shell ZnSe/ZnS QDs (Figure 1f).[18] Notably, a nonvolatile resistive switching memory based on type-I core–shell CdSe/CdS QDs was reported to process the durable and reproducible switching characteristics.[27]

Hybrid material systems containing QDs are often exploited to develop the effective memory components.[28,29] Wang et al. fabricated artificial photonic synaptic transistors by constructing the type-II heterostructure between the cesium lead bromide perovskite ($CsPbBr_3$) QDs and the organic semiconductor layer.[30] Usually, $CsPbBr_3$ QDs were synthesized through the hot-injection method[31] and then followed by solution processes for further utilization. With a flash memory operating mode, the $CsPbBr_3$ QDs layer is capable of trapping electrons and thus tuning the conductivity (or weight) of the synaptic device. The corresponding hypothesis is supported by the in situ Kelvin probe force microscopy (KPFM). Importantly, the optical potentiation and electrical habituation are implemented to realize various synapse functions that emulates the synaptic connection regulation in the human brain, including short-term, long-term, and spike-rate-dependent plasticity events.

Recently, tunable memory characteristics with multiple storage states have been realized in the hybrid black phosphorus (BP) QDs-based resistive random access memories (RRAMs).[29] In this work, self-assembled BP QDs were embedded in poly(methyl methacrylate) layers, acting as an active layer, which for the first time demonstrated the RRAMs based on BP QDs-polymer hybrid structure. Impressively, a high switching ratio ($\approx 10^7$) was demonstrated in such printed sandwiching multi-level RRAM, enabled by charge trapping in QDs. In another work, with a memristor structure, by introducing cerium dioxide (CeO_2) QDs as surface charge trappers directly onto the vertical zinc oxide (ZnO) nanorod arrays, their resistive switching performance was found to be significantly improved with the higher on/off ratios, the better device uniformity, and a long retention time over 10^4 s.[32]

In addition to the utilization of semiconducting QDs, artificial synapses can also be constructed by mixing metal nanoparticles into organic/inorganic films. For instances, Au and Ag nanoparticles assembled in pentacene films and SiO_x films, respectively, have been exploited for the fabrication of synaptic devices.[28] As a result of the tradeoff between surface tension and electric field, the dynamic retraction of Ag nanoparticles would result in the effective brain-like learning behaviors.

2.2. 1D Quantum Materials for Artificial Synapses

The topological resemblance of 1D materials to biological tubular axons have motivated their neuromorphic applications.[36] To date, 1D material technology has been proven to have a number of advantages in terms of carrier transport, energy efficiency, flexibility, scalability, and device miniaturization that usually outperform the other counterparts.[37–40]

One of the most extensively investigated 1D nanomaterials are the CNTs because of their high charge carrier mobility and highly-favorable solution-processability.[41,42] Till now, both aligned arrays and random networks of CNTs have been used to construct synaptic transistors. At the same time, the underlying device operating mechanisms with detailed characterizations, including floating gate, charge trapping, ion-migration, and electric double-layer effects, have been proposed. The global gate structure of CNT synaptic transistors could give rise to the local electric fields, which could overcome the activation energies for deep-level charge trapping. In addition, CNT channels could be doped into p-type or n-type via electrode engineering or surface doping approaches; therefore, they were capable to be fabricated into complementary inverters. The complementary inverters or circuits generally show the lower energy consumption and the easier integration when compared to the competing routes, while the same rules work well in existing synaptic transistors and circuits.[43,44] Recently, aligned CNT synaptic transistors with self-aligned T-gate structure has facilitated the micrometer-level scaling and the high-speed microsecond-level synaptic activities (**Figure 2**a), which benefits the future development of large-scale complementary metal-oxide-semiconductor (CMOS)-compatible neuromorphic computing systems.[33] Owing to the sturdiness of the aligned CNT synaptic transistors, a large dynamic range of conductance was effectively tuned by utilizing potentiating and depressing voltage pulses. Evidently, unsupervised pattern recognition tasks were realized in spiking neural networks (Figure 2b), showing great potential in the hardware implementation of CNT synaptic transistors.[33] However, the gate-bias-dependent charge trapping mechanism enables the synaptic transistors with fast operation, but lack of the non-volatile memory characteristics. One possible solution is to integrate CNT synaptic transistors with metal oxide memristors in a vertical architecture to bypass this problem.

Semiconducting NWs is another broad class of 1D materials. Early neuromorphic studies on group-IV and III-V semiconducting NWs, including Si, InP, and GaN, have demonstrated the non-volatile memory behavior by decorating redox active molecules on the NW surface (Figure 2c,d).[34] Various redox active molecules, such as ferrocene, zinc tetrabenzoporphine, and cobalt phthalocyanine (CoPc), were studied to realize efficient charge storage, non-volatile memory, and programmable logic functions on these NW devices. In particular, CoPc-functionalized InP NWs device arrays exhibited the excellent device performance with a current on/off ratios over 10^4, a retention duration above 20 min, and the independently addressability (Figure 2e).[34] Although the molecule-decorated

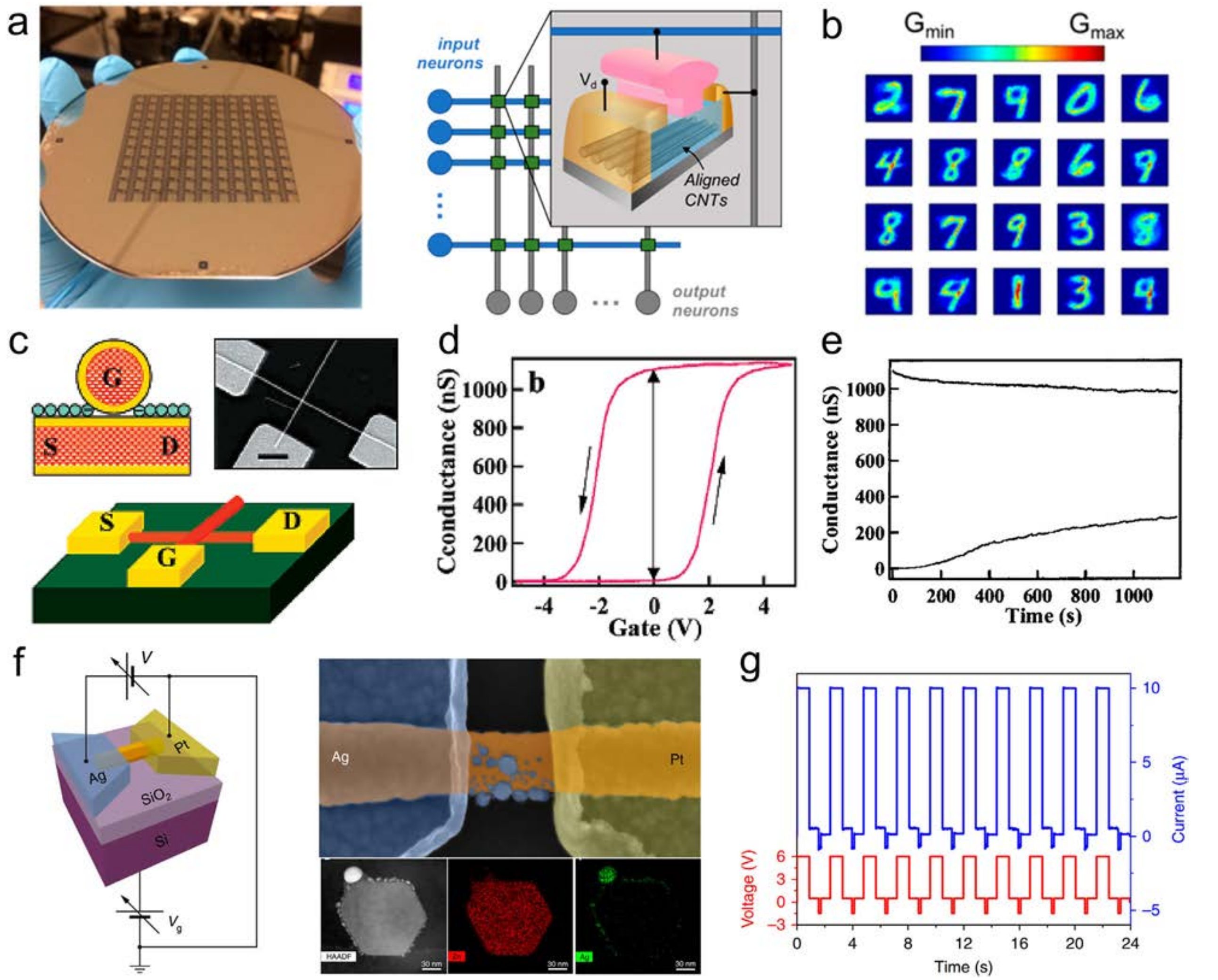

Figure 2. 1D quantum materials for artificial synapses. a) Highly aligned CNT synaptic transistor arrays at wafer level using the device structure of self-aligned T-gate. b) Unsupervised pattern recognition using spiking neural networks with aligned CNT synaptic devices. Reproduced with permission.[33] Copyright 2018, American Chemical Society. c) Semiconductor NW nonvolatile transistor devices functionalized with redox active molecules. d) Transfer curves of CoPc-functionalized InP NW-based nonvolatile devices with large hysteresis. e) Non-volatile memory based on CoPc-functionalized InP NW. Reproduced with permission.[34] Copyright 2002, American Chemical Society. f) Schematic diagram and false-color SEM image of single ZnO NW-based memristive device contacted by Ag/Pt electrodes. Inset shows the reorganization of the Ag nanoclusters distributed on the NW surface. g) Non-volatile resistive switching behaviors of single ZnO NW with reliable SET (6 V, 880 ms pulse) and RESET (−1.5 V, 180 ms pulse) processes. Reproduced under the terms of a Creative Commons Attribution 4.0 License (CC BY).[35] Copyright 2018, The Authors, published by Springer Nature.

NW transistors were not connected to the synaptic devices in such the earlier work, this demonstration obviously pave the way to utilize molecular NW electronics for advanced neuromorphic applications.

Since then, various metal oxide semiconductor NWs have been explored for different neuromorphic applications, for example, ZnO, TiO_2, CuO_x, NiO, Zn_2SnO_4, and Ga_2O_3.[45–48] Due to the generally wide bandgap, the metal oxide NWs show the high photo-sensitivity to UV region,[46,49] which could function as building blocks for photonic synaptic devices.[50] In these cases, the interaction of simultaneous light pulses with adsorbed and bulk oxygen in the surface depletion region play a key role in regulating the NW conductance, that is, the synaptic weight.[9,51] In a recent work, both volatile and non-volatile resistive switching have been achieved in Ag-contacted ZnO nanowire devices, mainly enabled by the atomic Ag diffusion along the NW (Figure 2f,g), which well emulate the ion migration dynamics in biological synapses.[35] With detailed investigation of the memristive mechanism in the Ag–ZnO system, the underlying electrochemical fundamentals of filament formation/dissolution highlight the Ag^+/Ag redox reactions and transport characteristics on the crystalline NW surface. These observations reveal the importance of surfaces and interfaces in single-crystalline NWs to realize the artificial redox-based NW synapses. In a hybrid 1D-0D system, vertically aligned ZnO NWs decorated with CeO_2 QDs have been employed to configure memristors based on charge trapping mechanisms.[32]

Organic core–sheath PEO-P_3HT NWs with a nerve fiber-like morphology were fabricated to resemble the biological ion channels and emulate the corresponding synaptic functions.[36] When weak pre-synaptic spikes are applied, the electrolyte ions would diffuse into the PEO sheath after stimulation and then these ions diffuse back quickly, resulting in the short-term potentiation. In contrast, the intense stimulation could drive the ion penetration further into the core of P_3HT, which adds a high barrier to the reverse ion diffusion, yielding the long-term potentiation. Impressively, the exceptional low energy consumption per synaptic event of ≈1.23 fJ was obtained, rivaling that of the biological synapses (≈10 fJ per event) and the most reported artificial synapse devices. In a possible hypothesis, the electrolyte ions penetrated to the NW surface or deeper into the polymer shell would result in large electronic double-layer capacitances, which accounts for the ultralow power per synaptic event in such organic core-shell NWs. With similar principles, an organic electrochemical transistor exhibited 500 distinct conductance states within a narrow range of only 1 V, together with a low energy consumption of ≈10 pJ per event.[52] It is worth noting that the polymer electrolytes could create a common electrochemical environment, which allowed electrochemical devices coupled with the multiple terminal gating. The spatially distributed inputs (i.e., gating) could then imitate the homeoplasticity of truly biological-like neural networks.[53,54]

2.3. 2D Quantum Materials for Artificial Synapses

Within recent two decades, 2D materials have provided remarkable mechanical and electrical properties as well as improved device integration with planar wafer technologies.[13,61,62] Also, the rich variety of electrical/chemical properties of 2D materials have given them the unexpected neuromorphic functionality, which subsequently facilitates the development of novel computing devices.[8,63,64]

Sub-nanometer ultrathin vertical memristors are lately manufactured by sandwiching monolayer TMDCs (MX_2, M = Mo, W; X = S, Se) between Au electrodes (**Figure 3**a).[55,65] Governed by the point defects in monolayer semiconductors, a high switching ratio of over 10^4 together with a high-frequency switching at 50 GHz were obtained (Figure 3b).[55] The Au electrodes could also be replaced by the graphene layers to form van der Waals contacts. The dangling bond-free and defect-free electrical contacts is an essential requirement to be capable to operate in harsh environments, for instance, operating at a high temperatures of 340 °C that is higher than traditional metal-oxide memristors of ≈200 °C.[66] The potential operation mechanism in 2D materials-based memristors that involving the formation/filling of sulfur vacancies has been proposed and experimentally proved by in situ microstructural characterizations and conductive atomic force microscopy (Figure 3c).[55] Electrode engineering was also integrated with ultrathin vertical 2D memristors to enhance the device performance. For example, in a Cu/bilayer MoS_2/Au memristor, the low switching voltage (<0.25 V) and the first demonstration of spike-timing dependent plasticity (STDP) in 2D memristors were reported (Figure 3d,e), in which the Cu ion diffusion through point defects plays the key role.[56] In addition to the semiconducting 2D materials, insulating few-layer hexagonal boron nitride (h-BN) have also combined with active Cu or Ag metals to demonstrate the bipolar and unipolar resistive switching (Figure 3f).[57,63]

In the lateral device geometry, diverse neuromorphic functionalities have been demonstrated based on 2D materials, including graphene, graphene oxide, TMDCs, etc. For example, twisted bilayer graphene is utilized to fabricate synaptic transistors with tunable plasticity, which is highly related to the oxygen ions and vacancies in AlO_x dielectrics.[67] Owing to the ambipolar feature of graphene, both excitatory and inhibitory behaviors could be achieved in a single device to mimic the multi-level dynamics of biological synapse. By varying carrier density of graphene, Hebbian learning and STDP are well demonstrated and controlled by gate voltage polarity. Moreover, taking advantages of the in-plane reversibly diffusion of lithium ions (Li^+) among the layers of few-layer graphene, the resulted electrochemical graphene artificial synapses show the high energy efficiency less than 500 fJ per event, the multi-state memory ability above 250 states, and a linear symmetric resistance response.[68] In addition, a planar device based on graphene oxide (GO) is fabricated by dripping the homogeneous GO solution on SiO_2 substrates.[69] Such planar Au/GO/Au devices displayed centrosymmetric non-zero-crossing hysteretic current-voltage characteristics, which is in a distinct contrast to the normal pinched hysteresis loop in most reported works. This could be ascribed to the migration and accumulation process of multiple ions within GO, such as H^+, SO_4^{2-}, and OH^-. These unique multiple polarization characteristics qualify the GO material being a distinctive material for the specific signal regulation in future neuromorphic computing. Based on the abundant ion migrations in GO, metal oxide thin-film synaptic transistors coupled by proton-conducting GO electrolytes have been assembled on flexible poly(ethylene terepthalate) (PET) substrates.[70]

Apart from the carbon-based 2D materials, layered TMDCs and BP have also been intensively explored in synaptic transistors using ionic motion. For instance, an in-plane ionic gating-modulated synaptic transistor based on few-layer WSe_2 was fabricated, which yields a dramatically lower energy consumption of ~30 fJ per event than that of graphene-based artificial synapses.[71] Interestingly, through detailed microstructural analysis and calculations, surface adsorption and internal intercalation of Li^+ lead to the different stimulation diffusive dynamics, causing short-term and long-term plasticity, respectively. Integrating several functionalities into the single artificial synapse could simplify the neuromorphic circuit design and bypass the process complexity. John et al. reported the electronic-ionotronic-photoactive MoS_2 synaptic devices that could respond to multiple stimuli, including electrical, ionic, and optical stimuli (Figure 3h).[59] Enabled by rich oxide traps and post-growth defect engineering of MoS_2, multi-level memory and on-demand symmetric and asymmetric Hebbian learning have been effectively demonstrated in 2D synaptic transistors. Most recently, taking utilization of the intrinsic polarity of two-dimensional materials, that is, ambipolar WSe_2, p-type BP, and n-type MoS_2, Chen et al. demonstrated the neuristors that could efficiently perform logic operations in a single synaptic device.[72] To highlight the potential of such kind neuristors, logic half-adder and parity-checker circuits as well as binary neural networks were constructed, which shows advantages in area saving and energy efficiency when compared to those in traditional design.

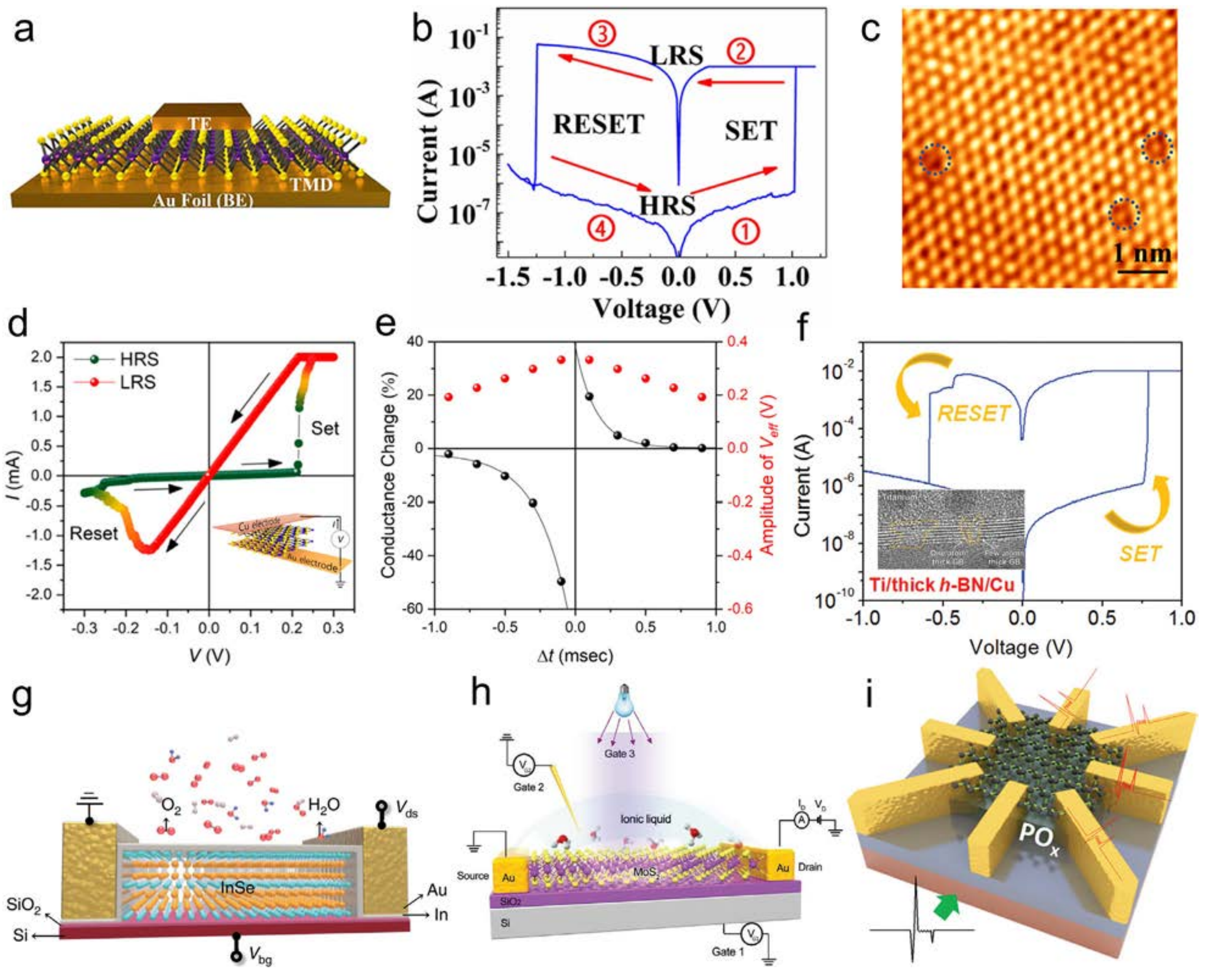

Figure 3. 2D quantum materials for artificial synapses. a) Device schematic of sub-nanometer ultrathin TMDCs vertical memristors based on the Au growth substrate. b) Typical bipolar resistive switching curve of the vertical monolayer MoS_2 memristor. c) STM images of the monolayer MoS_2 with S vacancy defects that marked by the dashed circles. Reproduced with permission.[55] Copyright 2018, American Chemical Society. d) Bipolar resistive switching curve of the Cu/bilayer MoS_2/Au memristor with a set voltage of 0.25 V and a reset voltage of −0.15 V. e) Spike-timing dependent plasticity (STDP) demonstrated in the bilayer MoS_2 memristors. Reproduced with permission.[56] Copyright 2019, American Chemical Society. f) Typical resistive switching behavior of the Ti/thick h-BN/Cu vertical memristor. Inset shows the cross-sectional HRTEM of h-BN with defective leaky paths. Reproduced with permission.[57] Copyright 2017, Wiley-VCH. g) Native oxidation events mediated ultrasensitive van der Waals materials (e.g., InSe and black phosphorus) for efficient neuromorphic computing devices. Reproduced under the terms of a Creative Commons Attribution 4.0 License (CC BY).[58] Copyright 2020, The Authors, published by Springer Nature. h) Synergistic electronic, ionotronic, and photoactive operation modes of the MoS_2 synaptic devices. Reproduced with permission.[59] Copyright 2018, Wiley-VCH. i) Black phosphorus-based synaptic transistor with the in-plane anisotropic electronic properties. Reproduced with permission.[60] Copyright 2016, Wiley-VCH.

Strong in-plane anisotropic electronic properties are generally observed in TMDCs and BP, potentially enabling anisotropic synaptic responses. Tian et al. fabricated the BP-based synaptic transistor for the first time, in which the crystal anisotropy of BP determines the in-plane anisotropic electronic properties, while the native phosphorus oxides (PO_x) are accounting for the synaptic characteristics (Figure 3i).[60] The natural oxide/2D semiconductor heterostructures are ideal for building synaptic devices. Most recently, native oxidation-induced charge trapping was also used to modulate the electronic properties of the InSe channel, to develop brain-like learning and memory abilities. With a thin and uniform indium oxides (InO_x) layer on the InSe layer, essential synaptic functions and reliable programming/erasing operations were emulated. At the same time, the pattern recognition simulation was successfully achieved based on the designed artificial neural network (Figure 3g).[58] These works reveal that the native oxidation events in van der Waals electronics is promising to establish efficient neuromorphic computing systems.

The concept of grain boundary engineering was also employed to modulate the memristive switching characteristics of gate-tunable memtransistors using polycrystalline CVD-grown monolayer MoS_2 as channels.[64] With a scalable fabrication process, conventional neural learning behavior as well as gate-tunable heterosynaptic functionality were achieved in a six-terminal MoS_2 memtransistor, together with large current on/off ratios, reliable resistive switching, and long-term retention. Through in situ experimental and device modelling studies, the resistive switching is mainly arising from the bias-induced movement of MoS_2 defects and the corresponding dynamically varying Schottky barrier heights. The seamless integration of multi-terminal device MoS_2 memtransistors with clear defect kinetics open the door to the experimental realization of complex neuromorphic learning based on 2D material systems. Besides the utilization of native defect, different postgrowth defect engineering methods, for instances, using helium-ion or electron-beam irradiation, have as well shown great promise for modulating the electronic properties and developing unique synaptic applications of 2D layered semiconductors. In particular, Jadwiszczak et al. utilized the focused helium ion beam to generate nanoscale defect-rich region on lateral monolayer MoS_2 memtransistors.[73] Subsequently, the helium-ion induced defects could be reversible drifted via applied electric field, leading to the modification of channel conductance and versatile memristive functionality.

For 2D nanomaterials, there also have some emerging resistive switching concepts, for examples, atom resistive switches and quantum phase transitions.[74] In 2008, a robust graphene-based atomic switches was reported for further nonvolatile information storage that is capable of reliable switching and long-time retention.[75] The authors proposed a memristive switching model based on the electric-field-driven formation/breaking of atomic carbon chains. Multiple chains could bridge the gap under strong electric field. The observed conductance steps of $\approx 2e^2/h$ is consistent to the theoretical calculations, which means that these carbon chains are metallic without significant Pierls distortion.[76] TMDCs have different crystalline phases, by which they exhibit varied semiconducting, semimetal and metallic properties.[74,77] Recently, Zhang et al. experimentally demonstrated the electric-field-induced structural transition in a vertical $MoTe_2/Mo_{1-x}W_xTe_2$ RRAM using metal or graphene as electrodes.[78] Reversible structural transitions among 2H semiconducting, distorted transient $2H_d$ structure, and orthorhombic T_d conducting phase of TMDC layers could be obtained after applying the appropriate electrical field. Impressively, the effective set pulse width of 10 ns is able to produce reproducible resistive switching between high and low resistive states. To limit the device current, $Al_2O_3/MoTe_2$ stack was also used in this work; as a result, a high current on/off ratios of 10^6 and a low programming currents of lower than 1 μA were obtained. This work illustrates the possibility to redefine the resistive switching of TMDC layers via electric field-induced selectively phase transitions. On the other hand, field-driven Li^+ ion intercalation was as well used to initiate 2H(semiconductor)–1T′(metal) phase transitions in few-layer MoS_2.[79] The local dynamically varying ion density plays a crucial role in the reliable synaptic competition and the cooperation of multi-terminal Li_xMoS_2 devices. Such coupled ionic-electronic strategies can be applied to other 2D materials, which generally have highly anisotropic ionic transport properties, offering advantages to future artificial neural networks in terms of controllability, power consumption, and process complexity.

Notably, local Joule heating effects have also been explored to encode the precise temporal information for sound localization, enabled by the thermal-induced metal–insulator transition in monolayer MoS_2.[80] In the same work, the unique metal–insulator transition process allows the ultralow operation power down to 10 fJ, comparable to the biological energy consumption. With a conductance threshold switching mechanism, heat is generated with electric current flowing through the channel, while in turn induces the metal–insulator transition. When a bias voltage lower than threshold value is used, the channel conductance could recover its initial state as a result of heat release. The similar temperature-resistivity relation was also applied on the chemical vapor deposition (CVD)-grown monolayer MoS_2 with different doping levels to demonstrate excitatory and inhibitory synaptic behaviors.[81]

2.4. Quasi-2D Electron Gases Interfaces for Artificial Synapses

Recently, fascinating quantized physical properties have been shown in complex oxide materials arising from strong carrier quantum-confinement effects.[82,83] After intensive investigations, it becomes clear that quasi-2D electron gases (quasi-2DEGs) formed at these heterointerfaces is the key to uncover these emergent phenomena.[84–86] More importantly, strong electron correlations in these atomically abrupt oxide heterointerfaces make quasi-2DEGs to be highly susceptible to fine control parameters, such as electric field, magnetic field, or light irradiation.[83,84,87] Interactions between these quasi-2DEGs and control parameters would create optoelectronic devices with tunable properties, e.g., non-volatile resistive switching,[88] ultrasensitive potentiometric bio-sensing,[89] and giant persistent photoconductivity.[90] Given high carrier mobility together with high sensitivity to various stimuli, quasi-2DEGs systems may enable more accurate probing of complex biological dynamics than that can be achieved by other material systems.[9,91]

Lately, Dror Miron et al. demonstrated a non-volatile resistive switching device based on quasi-2DEGs established between the $SrTiO_3$ substrate and the amorphous Al_2O_3 layer.[88] The oxygen vacancies from the $SrTiO_3/Al_2O_3$ conductive interface could drift into (out of) the Al_2O_3 layer under negative (positive) bias, leading to the formation (breakage) of the conductive filament. Here, oxide 2DEGs can serve as a reservoir of oxygen vacancies for non-volatile resistive storage, highlighting a simple and scalable route for future memory or neuromorphic devices. Moreover, Cen et al. reported the electric-field-induced creation of nanoscale conducting quasi-2DEGs regions at $SrTiO_3/LaAlO_3$ interfaces, which is on the basis of metal–insulator quantum phase transition.[92] Reversible localized metal–insulator transitions have a featured length scales below 5 nm, while the patterned conducting structures show a long storing duration more than 24 h. Reversibly nanoscale patterning of high-mobility quasi-2DEGs gives great opportunities to explore high-performance information processing and ultrahigh-density information storage.

Furthermore, an unprecedented persistent photoconductivity (PPC) effect was found at $SrTiO_3/LaAlO_3$ interfaces by Tebano et al.,[90] where light-induced giant conductivity was measured to increase by five orders of magnitude. The long-duration persistence (>24 h) and the giant value of photocurrent at the $SrTiO_3/LaAlO_3$ interfaces is much larger than those reported values. A connection between giant photoconductivity and quasi-2DEGs was proposed to qualitatively explain such phenomenon, in which the energy band structure of quasi-2DEGs could efficiently separate the photo-generated carriers and thus significantly enhance the interfacial conductance. The PPC effect in

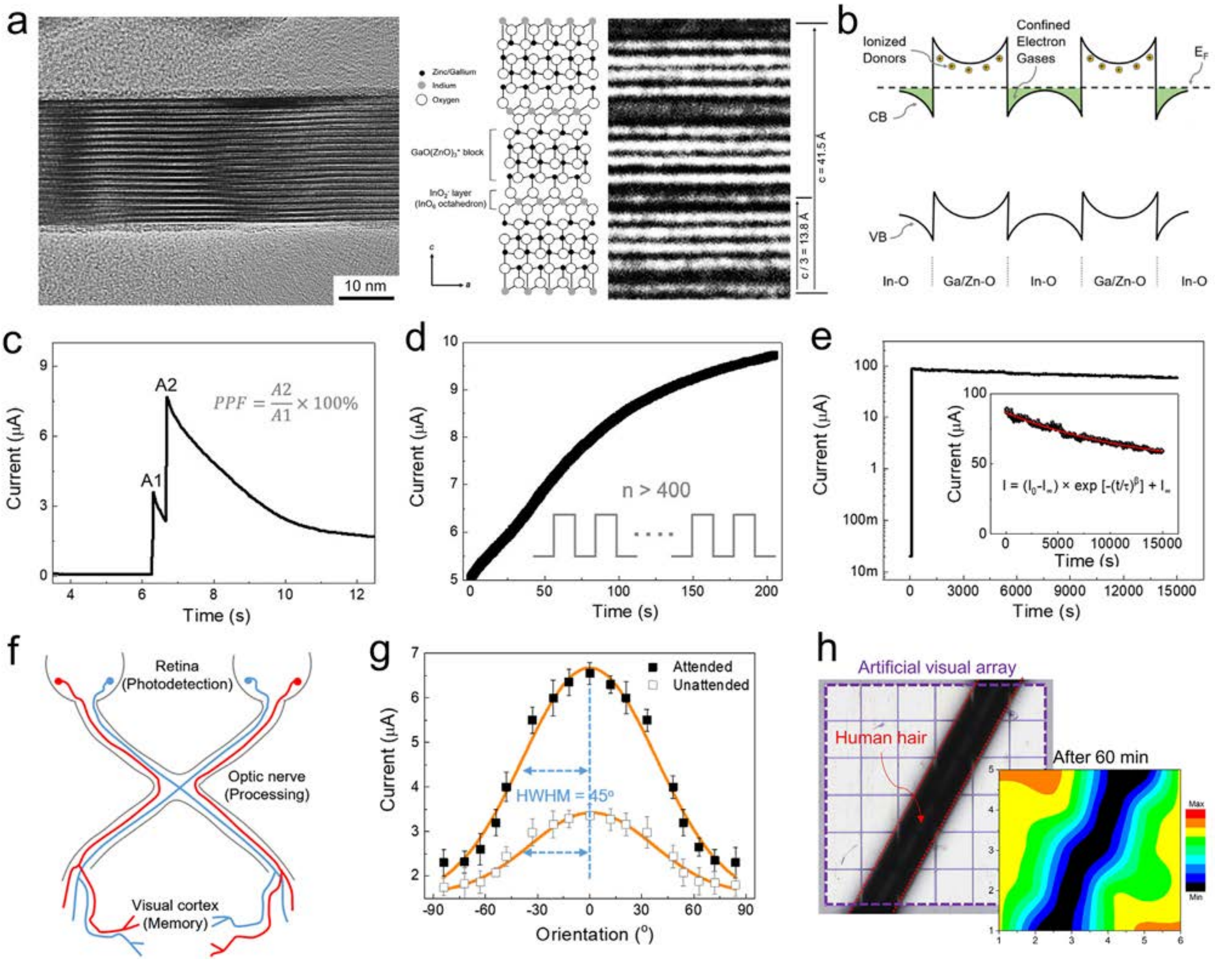

Figure 4. Quasi-2D electron gases interfaces for artificial synapses. a) HRTEM images of $InGaO_3(ZnO)_3$ superlattice NW with alternating stacks of InO_2^- layers and $GaO(ZnO)_3^+$ blocks. b) Energy-band structure of quasi-2DEGs in the $InGaO_3(ZnO)_3$ superlattice. c) Paired-pulse facilitation, d) multi-bit storage, and e) nonvolatile charge retention properties of quasi-2DEG photonic synaptic device. f) Schematic diagram of the human visual system, consisting of retina (visual detecting), visual nerve (information processing), and primary visual cortex (image memory). g) Attended/unattended orientation selectivity and h) image memorizing behaviors of quasi-2DEG artificial visual system. Reproduced with permission.[9] Copyright 2020, The Authors, some rights reserved; exclusive licensee AAAS. Distributed under a Creative Commons Attribution NonCommercial License 4.0 (CC BY-NC).

quasi-2DEGs interfaces could open new perspectives for creating new optoelectronic devices. For example, using the similar $SrTiO_3/LaAlO_3$ heterojunctions, Irvin et al. have developed rewritable nanoscale photodetectors that are electric field-tunable and could work over the visible-to-near-infrared regime.[87] Solar-blind UV sensitive PPC was also reported on $SrTiO_3/LaAlO_3$ heterojunctions, arising from photo-induced electron migrations from oxygen defects to interfaces.[93]

Oxygen desorption could also alter the electrical properties of quasi-2DEGs interfaces. For instance, Meevasana et al. showed that the carrier density of a quais-2DEG can be controlled by UV light irradiation, which is due to the light-mediated oxygen desorption from the $SrTiO_3$ surface.[91] Through angle-resolved photoemission spectroscopy measurements, an unexpected concurrence of a light quasi-particle mass and signatures of intense many-body interactions were also identified. This also suggests that writing of surface states on the quasi-2DEG NW surface using light would be an active route to efficiently program their conductivity. Other than oxide interfaces, group III-V heterojunction interface of AlGaN/GaN was also observed to possess PPC effect by Li et al.[94,95] The photoionization of deep level defects in the AlGaN barrier was believed to be the main reason for the observed photo-induced increase of 2DEG carrier density and mobility (up to 5800 $cm^2\ V^{-1}$ at 10 K).[94] The corresponding energy barrier is quantitatively estimated to be 230 meV, which is efficient to confine photo-generated electrons in the 2DEG channel.

Most recently, Meng et al. demonstrated the quasi-2DEGs photonic synapses based on $InGaO_3(ZnO)_3$ superlattice NWs (**Figure 4**a), by utilizing an unreported device operation concept, which combines the oxygen adsorption-desorption kinetics on NW surface and the strong quantum-confinement effects of carriers in superlattice cores (Figure 4b).[9] These devices duplicate the Ca^{2+} ion flux and neurotransmitter release characteristics in biological synapses. Importantly, these quasi-2DEGs photonic synapses can precisely define their conductance state (or synaptic weight) for emulating synaptic behaviors (Figure 4c–e), which shows the bionic performance that is unreachable by other conventional materials. Recorded ultralow energy consumption down to sub-femtojoule (0.7 fJ) per synaptic event is obtained in quasi-2DEGs synapses, which outperforms the biological synapses (≈10 fJ per synaptic event). The unique multiple quantum well structure of quasi-2DEGs superlattice NWs is the main reason for this technological breakthrough. Notably, a flexible quasi-2DEGs artificial visual system is demonstrated that can simultaneously execute high-performance photodetecting, in-memory data processing (Figure 4c), multiple-state memory (with 400 distinct programmable states, Figure 4d), non-volatile information retention (Figure 4e), orientation selectivity (Figure 4g), and image memorization (Figure 4h).[9]

In biological visual systems, orientation selectivity is a well-known function of the primary visual cortex that is necessary for the encoding of visual images. In the work by Meng et al., orientation selectivity is fully experimentally demonstrated on a real moving object, where visual responses of the quasi-2DEGs photonic synapses were measured in both "attended" and "unattended" modes (Figure 4g).[9] Although the output synaptic signals of devices were suppressed in "unattended" mode, its orientation selectivity that determined by the orientation-tuning curve does not get obviously altered. The illustration of the superior orientation selectivity in quasi-2DEGs devices is meaningful to the hardware visual information detection and processing.

3. Quantum Effects in Artificial Synapses

3.1. Josephson Junction-Based Artificial Synapses

Josephson effect, an kind of macroscopic quantum phenomenon, could be exploited to construct ultralow power artificial synapses.[102] In a recent paper, Schneider et al. fabricated artificial synaptic devices based on Josephson junctions with embedded magnetic Mn nanoclusters.[96] The spin states of Mn nanoclusters resemble the neurotransmitter dynamics in the biological system. The overall magnetic order of Josephson junctions could be modulated by altering the net spins of Mn nanoclusters (**Figure 5**a), which in turn tunes the critical current (i.e., synaptic connection strength).[96] Impressively, on the basis of the reconfigurable magnetic Josephson effect, an ultralow spiking energy less than 1 aJ per synaptic event and a Josephson plasma frequency exceed 100 GHz were obtained in this artificial synapse. By the same group, single flux quantum based neuromorphic computing was also demonstrated on Josephson junction with a superconductor–insulator–superconductor structure of Nb/AlO_x-Al/Nb.[103] Most lately, fully coupled randomly disordered recurrent superconducting synaptic networks that constructed on Josephson junctions were proposed to enable the unsupervised learning.[104] The hybrid magnetic/superconducting technologies based on Josephson junctions combined with natural plasticity behaviors have great possibility to become faster and to consume less energy as compared with the implemented software-based or hardware-based spiking networks. In addition to operating speed and energy consumption, Josephson-junction-based neuromorphic technology is more suitable to highly complex recurrent networks, beyond currently existed feed forward networks.[105]

3.2. Artificial Synapses Using Quantum Tunneling Effect

Enabled by quantum tunneling effect, the electrons could propagate through an energy barrier even if the electron energy is less than the barrier height. Taking advantages of quantum tunneling effect, many advanced electronics with performance breakthroughs are made to date, such as tunneling diodes[106–108] and tunneling field-effect transistors.[109,110] Just now, tunneling effect was also introduced into synaptic devices. For instance, Paul et al. reported a charge-tunneling enabled synaptic transistor utilizing ultrathin MoS_2 as the channel and h-BN as the tunneling barrier.[97] Given by tunneling effect and high gating efficiency, the resulted floating-gate device exhibited a near-ideal sub-threshold swing down to 77 mV per decade. The h-BN barrier layer could efficiently control the electron tunneling into graphene floating gate, which thus tunes the channel conductance for mimicking various synaptic plasticity with desirable high energy efficiency (Figure 5b).[97] In addition, with a double floating gate device configuration, superior linearity and symmetry in bidirectional conductance change curves were found in MoS_2 flash memory devices.[111] Highly controllable electron tunneling and injection in these double floating gated devices is the main reason of the symmetry of potentiation and depression processes, and ultimately beneficial to the demonstration of various synaptic functions. Also, a semi-floating gate tunneling transistor based on band-engineered WSe_2/MoS_2/HfS_2 heterostructures was reported to show the greatly enhanced 10 nanosecond-level writing speed, which is ≈10^6 times than other 2D material-based memories and close to the commercial dynamic random access memory (DRAM) technology.[112] Solid-state synaptic devices based on tunneling effects have advantages over other neuromorphic designs because it is free of defect generation and ion movement, thus offering a faster and more robust platform for future neuromorphic hardware applications. Most recently, an ultrafast flash memory based on van der Waals heterostructures of MoS_2/h-BN/graphene was demonstrated, by which a device writing/erasing speed down to 20 ns was achieved.[113] After detailed experimental and theoretical analysis, tunneling barrier, gate coupling, and van der Waals interface were proved to be the main factors for the realization of breakthrough operating speed.

3.3. Spintronics-Based Neuromorphic Components

Spintronics are constructed from the spin property of an electron, instead of its charge in conventional electronics.[114] Recently, spintronics-based devices have gained significant interest as promising building blocks for next-generation neuromorphic computing components, mainly driven by their low energy consumption, fast switching, and highly stable/reproducible operation.[115] For example, magnetic domain walls-based neuromorphic components have been reported to be capable of multi-level linear synaptic weight generator and nonlinear thresholding (Figure 5c).[98] Impressively, with a micrometer-size device dimension and 8 ns current pulses, the ultralow

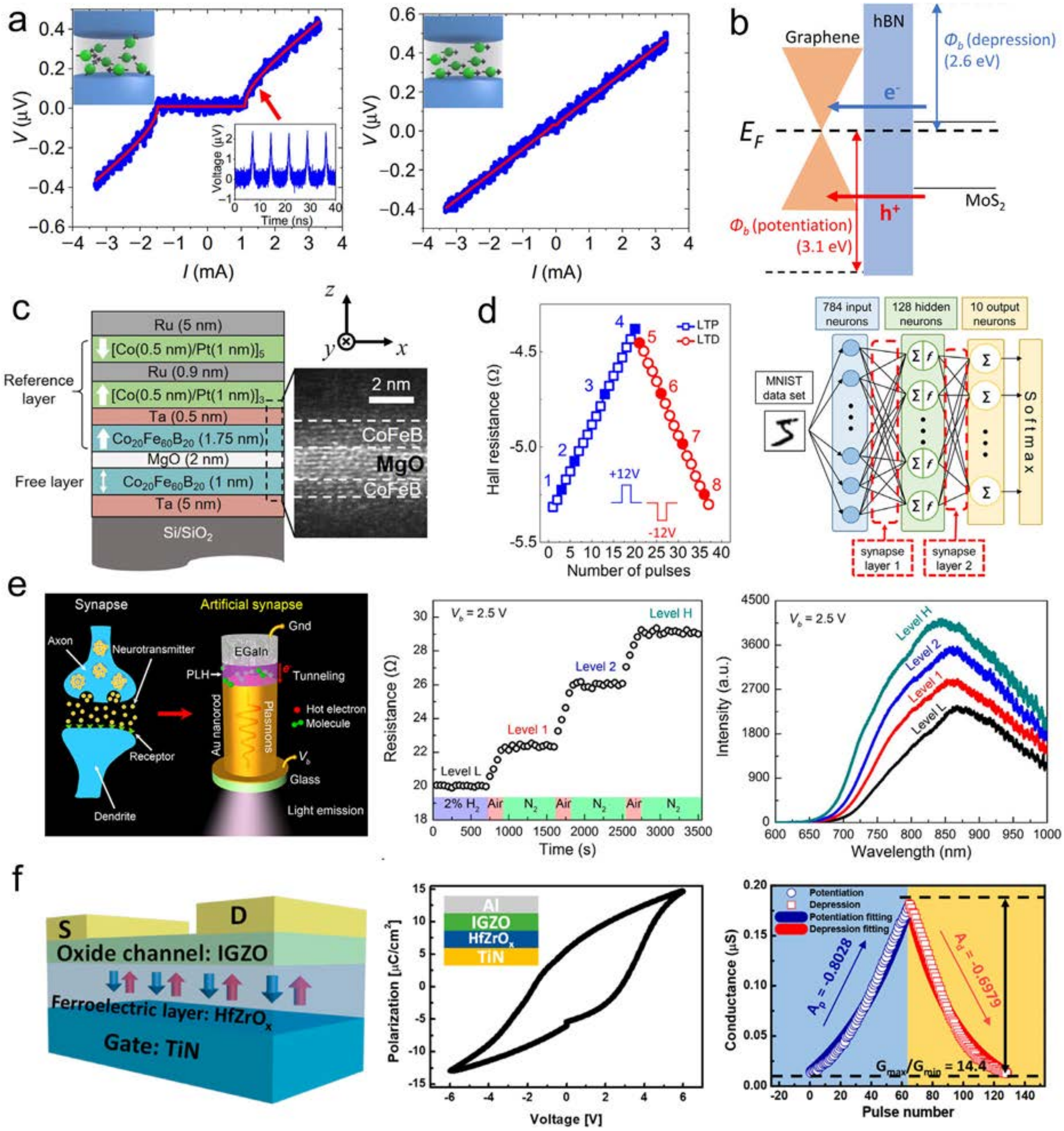

Figure 5. Quantum effects in artificial synapses. a) Magnetically disordered state (left) and the magnetically ordered state (right) of Josephson junction-based artificial synapses. Reproduced with permission.[96] Copyright 2018, The Authors, some rights reserved; exclusive licensee AAAS. Distributed under a Creative Commons Attribution NonCommercial License 4.0 (CC BY-NC). b) Energy-band diagram of charge-tunneling based synaptic transistor using ultrathin MoS_2 as the channel and h-BN as the tunneling barrier. Reproduced with permission.[97] Copyright 2019, IOP Publishing. c) Magnetic domain walls-based synaptic device with multi-level linear synaptic weight generator and nonlinear thresholding. Reproduced with permission.[98] Copyright 2019, American Chemical Society. d) Integrated multi-layer neural networks consisting of spintronics-based synapses and neurons. Reproduced under the terms of a Creative Commons Attribution 4.0 License (CC BY).[99] Copyright 2021, The Authors, published by Springer Nature. e) Synapse-inspired hot-electron tunnel junction memristor showing programmable multi-level programming electrical and optical properties. Reproduced with permission.[100] Copyright 2020, American Chemical Society. f) Ferroelectric analog synaptic transistors based on $HfZrO_x$ ferroelectric dielectrics and InGaZnO channels showing linear potentiation/depression behaviors.[101] Copyright 2019, American Chemical Society.

energy consumption ranging between 1 and 16 pJ are sufficient to induce weight modulation. Both operation speed and energy dissipation are better than other synaptic nonvolatile memory devices. Importantly, the fabrication process of above mentioned spintronics-based synaptic devices are compatible with the available silicon processes. Besides, as a kind of nanoscale spin textures, magnetic skyrmions could be manipulated by electric current, which makes it another potential player to handle information processing and storage. For instance, Song et al. reported magnetic skyrmion-based artificial synapses for neuromorphic computing by manipulating Hall voltage output signals.[116] At room temperature, those skyrmions could be generated, moved, and deleted enabled by electrical pulses, mimicking the variations in synaptic weights to demonstrate biological potentiation and depression synaptic behaviors. In chip-level simulations, skyrmion-based neuromorphic system achieved a pattern recognition accuracy of ∼89%. In addition, a proof-of-principle neuromorphic computing networks using $MgO/Co_{20}Fe_{60}B_{20}/W$ spintronic devices were reported by Yang et al. most lately.[99] The integrated neural networks that consist of spintronics-based synapses and neurons were used to perform the typical pattern classification task, where an excellent classification accuracy over 93% was obtained. It would be meaningful to establish more compact and efficient spintronics-based neural network systems to realize diverse cognition functions.

3.4. Hot Electron Tunnel Junctions

Nonvolatile memristors have attracted extensive interest arising from their promises in next-generation signal processing and memorizing, in which the operation of memristors are mainly relying on two principles, that is, conductive filament formation and magnetic domain regulation. In specific, the electric field-induced formation or deformation of conductive filaments are developing as the rule mode of metal oxide-based RRAMs,[117,118] while magnetic tunnel junctions serve as the basis of spintronic-based magnetoresistive random-access memory.[119–121] Recently, multi-state resistance switching was explored in a metal–polymer–metal (i.e., eutectic gallium indium/poly-L-histidine/gold nanorod) plasmonic tunnel junctions (Figure 5e),[100] with a new principle based on hot-electron-mediated chemical reactions.[122] The hot electrons could be generated under electric field or light irradiation, allowing independent electrically or optically modulations in the same device.[100] The nonvolatile information memory in such hot electron tunnel junctions could be represented by electrical resistance or inelastic-tunneling-induced light emission.[123] Determined by the Au nanorod density, the plasmonic tunnel junctions may be configured into networks with a potential high density of $\approx 10^{10}$ cm^{-2}, in which single junction could be addressed individually if required. Apart from the application in traditional multi-level memristive devices, the demonstrated programmable tunnel junctions would be integrated with plasmonic or silicon waveguides to form artificial optoelectronic or photonic synapses for nonspiking artificial neural networks.[124,125]

3.5. Quantum Filamentary Conductance of RRAMs

Nanoscale filamentary switch represents the smallest memory element. However, limited by appropriate characterization techniques, it is difficult to identify the corresponding filamentary conductance quanta. Lately, detailed quantum characterization of such quantum filamentary conductance was directly investigated via superconducting subgap spectroscopy.[126,127] By applying this unique method, the transmission probabilities of the individual quantum conductance channels were studied to reveal the physical nature of filamentary conductance, showing more insights about the conduction properties of resistive switching devices.[126] In the same work, the high conductance state of Nb_2O_5 resistive switching junctions is experimentally proved to be arising from the formation of atomic-sized metallic filaments. A quantized conductance of $2e^2/h$ is the profound indication of atomic switching in filamentary RRAM units, which is also consistent with the reported silver-based atomic switches.[128,129] Filamentary switches with quantized conductance provide us an ultimately precise medium to process data more plastically and fault-tolerant, which potentially enables device down-scaling to the atomic scale.

3.6. Ferroelectric Synaptic Devices

Ferroelectric materials featured as spontaneous electrical polarization phenomenon, which could be reversed by an external electric field.[130] Owing to their reversible polarization and nonvolatile multilevel memory effect, ferroelectrics have been considered as promising candidates for synaptic devices using in hardware neural networks. Lately, inorganic hafnium-based oxides and organic poly(vinylidene fluoride/trifluoroethylene) [P(VDF-TrFE)] were used as ferroelectric dielectrics to fabricate ferroelectric field-effect transistors (FeFET). Kim et al. reported the analog conductance modulation behavior in the FeFET that was based on hafnium zirconium oxide ($HfZrO_x$) ferroelectric dielectrics and InGaZnO channels (Figure 5f).[101] Induced by the accurate polarization changes of $HfZrO_x$ ferroelectric layer, FeFET showed linear potentiation/depression characteristics, multiple memory states, and small cycle-to-cycle variations. Also, enabled by the linear and symmetric conductance modulation, artificial neural network based on the proposed FeFET was used to realize pattern recognition.[131] As a result, a pattern recognition accuracy of 84% was achieved, which shows that the ferroelectric synaptic devices are promising for high-density neuromorphic systems in the future. Apart from inorganic ferroelectrics, synaptic devices based on organic ferroelectrics were also investigated intensively.[132–134] By Wang et al., electrochemical synaptic transistor gated by P(VDF-TrFE) polymer dielectric was demonstrated to process non-volatile plasticity up to 10^4 s and unique threshold switching.[132] Utilizing such ferroelectric threshold property, an artificial visual-perception system was constructed to transduce light intensity and frequency information into analog synaptic signals, by which a primary color recognition function was obtained. In addition to FeFET, ferroelectric synaptic devices could be made in the forms of ferroelectric capacitor and ferroelectric tunnel junction (FTJ).[130,135] Note that among those device structures, FeFET has advantages in terms of scalability and CMOS compatibility, offering significant opportunities to realize ultralow-power hardware artificial neural networks.[131,134]

4. Outlook

As summarized in this review, low-dimensional quantum materials, including 0D, 1D, and 2D materials, have been widely studied in emerging neuromorphic devices and in-memory computing architectures. This is mainly powered by the unique properties of each kind of quantum materials. In specific, 0D quantum materials could be tailored by size, shape, surface ligand, chemical composition, and so on, giving rise to their strong quantum and dielectric confinement effects. With highly tunable electronic and optical properties of QDs, 0D materials-based neuromorphic devices become a powerful platform to demonstrate synaptic functions beyond conventional materials. Besides, 1D materials have topological resemblance to biological tubular axons, which motivate their neuromorphic applications. Benefiting from their intrinsic advantages in terms of carrier transport, energy efficiency, flexibility, scalability, and device miniaturization, 1D material-based neuromorphic devices usually outperform the other counterparts. Also, 2D materials and quasi-2DEGs interfaces, always associated with remarkable electrical properties and improved device integration with planar wafer technologies, show promising results on multiple terminal gating, in situ characterizations, and spatiotemporal synaptic responses. Apart from that, the rich physical/chemical properties of 2D materials and quasi-2DEGs interfaces will give them the unexpected neuromorphic functionality in the future.

With significant research efforts, a number of new quantum materials and impressive quantum effects have been explored, benefiting for fundamental science and practical applications in areas of electronics, photonics, optoelectronics, spintronics, and valleytronics. For instance, the emergence of layered magnetic insulators (e.g., CrI_3 and $CuCrP_2S_6$), ferroelectric semiconductors, and inorganic atomic chain (e.g., Te), provides the diverse possibilities of new device applications. Intrinsic 2D ferroelectric semiconductors are also attractive for synaptic device applications because of their vertical scaling feature and high carrier mobility. 2D ferroelectric semiconductors could be classified as in-plane family (e.g., SnS), out-of-plane family (e.g., 1T-$MoTe_2$), and intercorrelated family (e.g., In_2Se_3), where weak interlayer coupling endows their retentions of ferroelectric properties in nanoscale layered structure. Nevertheless, there are still numerous unexplored phenomena and inconsistencies in the existing quantum studies, which needs additional investigation for the subsequent development of high-performance neuromorphic devices.

Over the past decades, low-dimensional materials have been regarded as powerful platform to regulate the electrical, optical, magnetic, and thermoelectric properties of solid-state materials. Although the outstanding performances of low-dimensional materials suffice for most emerging applications, for example, the quantum artificial synapses highlighted in this review, their scalability and integration are not optimal for large-area applications. As results from assembly- and processing-related obstacles during the transfer process, for example, solution transfer process or contact transfer printing, the macroscale integration of low-dimensional materials is less effective. Moreover, lacking compatibility with arbitrary substrates and suffering from batch-to-batch variations are also challenging tasks for practical applications. To remove these serious constrains, new in situ fabrication methods of low-dimensional materials that equipping high-throughput and simple processing is highly desirable.

System-level demonstrations with high energy efficiency are the ultimate goals of neuromorphic computing technologies. To date, conventional silicon CMOS electronics have achieved remarkable progresses in system-level applications; however, it is still limited by the high computational power and low throughput of von Neumann computing architecture. Emerging neuromorphic in-memory computing devices, with merged data processing and memorizing units, are regarded as promising candidates for system-level hardware implementation. To realize system-level experimental verifications, there are many technical problems that need to be solved by cooperative research of different interdisciplinary fields, ranging from material synthesis, and device fabrication, all the way to algorithm design, architecture development, and circuit integration.

Acknowledgements

This work was supported by the Research Fellow Scheme (RFS2021-1S04) and the Theme-based Research (T42-103/16-N) of the Research Grants Council of Hong Kong SAR, China, and the Foshan Innovative and Entrepreneurial Research Team Program (No. 2018IT100031).

Conflict of Interest

The authors declare no conflict of interest.

Keywords

artificial synapses, in-memory computing, quantum effects, quantum materials

Received: May 29, 2021
Revised: August 11, 2021
Published online:

[1] E. R. Kandel, J. H. Schwartz, T. M. Jessell, D. o. Biochemistry, M. B. T. Jessell, S. Siegelbaum, A. Hudspeth, *Principles of Neural Science*, McGraw-hill, New York **2000**.
[2] B. C.-K. Tee, A. Chortos, A. Berndt, A. K. Nguyen, A. Tom, A. McGuire, Z. C. Lin, K. Tien, W.-G. Bae, H. Wang, P. Mei, H.-H. Chou, B. Cui, K. Deisseroth, T. N. Ng, Z. Bao, *Science* **2015**, *350*, 313.
[3] L. F. Abbott, W. G. Regehr, *Nature* **2004**, *431*, 796.
[4] Y. Kim, A. Chortos, W. Xu, Y. Liu, J. Y. Oh, D. Son, J. Kang, A. M. Foudeh, C. Zhu, Y. Lee, S. Niu, J. Liu, R. Pfattner, Z. Bao, T.-W. Lee, *Science* **2018**, *360*, 998.
[5] L. E. Osborn, A. Dragomir, J. L. Betthauser, C. L. Hunt, H. H. Nguyen, R. R. Kaliki, N. V. Thakor, *Sci. Rob.* **2018**, *3*, eaat3818.
[6] X. Zhang, Y. Zhuo, Q. Luo, Z. Wu, R. Midya, Z. Wang, W. Song, R. Wang, N. K. Upadhyay, Y. Fang, *Nat. Commun.* **2020**, *11*, 51.
[7] A. Sebastian, M. Le Gallo, R. Khaddam-Aljameh, E. Eleftheriou, *Nat. Nanotechnol.* **2020**, *15*, 529.
[8] C. Liu, H. Chen, S. Wang, Q. Liu, Y.-G. Jiang, D. W. Zhang, M. Liu, P. Zhou, *Nat. Nanotechnol.* **2020**, *15*, 545.
[9] Y. Meng, F. Li, C. Lan, X. Bu, X. Kang, R. Wei, S. Yip, D. Li, F. Wang, T. Takahashi, T. Hosomi, K. Nagashima, T. Yanagida, J. C. Ho, *Sci. Adv.* **2020**, *6*, eabc6389.
[10] L. Gu, S. Poddar, Y. Lin, Z. Long, D. Zhang, Q. Zhang, L. Shu, X. Qiu, M. Kam, A. Javey, *Nature* **2020**, *581*, 278.
[11] B. Tian, C. M. Lieber, *Chem. Rev.* **2019**, *119*, 9136.
[12] V. K. Sangwan, M. C. Hersam, *Nat. Nanotechnol.* **2020**, *15*, 517.
[13] Y. Yi, Z. Chen, X. F. Yu, Z. K. Zhou, J. Li, *Adv. Quantum Technol.* **2019**, *2*, 1800111.
[14] G. Milano, F. Ferrarese Lupi, M. Fretto, C. Ricciardi, N. De Leo, L. Boarino, *Adv. Quantum Technol.* **2020**, *3*, 2000009.

[15] M. C. Weidman, M. E. Beck, R. S. Hoffman, F. Prins, W. A. Tisdale, *ACS Nano* **2014**, *8*, 6363.
[16] B. C. Das, S. K. Batabyal, A. J. Pal, *Adv. Mater.* **2007**, *19*, 4172.
[17] J. Wang, Z. Lv, X. Xing, X. Li, Y. Wang, M. Chen, G. Pang, F. Qian, Y. Zhou, S. T. Han, *Adv. Funct. Mater.* **2020**, *30*, 1909114.
[18] Z.-P. Wang, Y. Wang, J. Yu, J.-Q. Yang, Y. Zhou, J.-Y. Mao, R. Wang, X. Zhao, W. Zheng, S.-T. Han, *Nano Lett.* **2020**, *20*, 5562.
[19] T. M. Zhao, Y. Chen, Y. Yu, Q. Li, M. Davanco, J. Liu, *Adv. Quantum Technol.* **2020**, *3*, 1900034.
[20] T. P. Osedach, N. Zhao, T. L. Andrew, P. R. Brown, D. D. Wanger, D. B. Strasfeld, L.-Y. Chang, M. G. Bawendi, V. Bulovic, *ACS Nano* **2012**, *6*, 3121.
[21] A. G. Shulga, S. Kahmann, D. N. Dirin, A. Graf, J. Zaumseil, M. V. Kovalenko, M. A. Loi, *ACS Nano* **2018**, *12*, 12805.
[22] C. H. Jo, J. H. Kim, J. Kim, J. Kim, M. S. Oh, M. S. Kang, M.-G. Kim, Y.-H. Kim, B.-K. Ju, S. K. Park, *J. Mater. Chem. C* **2014**, *2*, 10305.
[23] S. A. McDonald, G. Konstantatos, S. Zhang, P. W. Cyr, E. J. Klem, L. Levina, E. H. Sargent, *Nat. Mater.* **2005**, *4*, 138.
[24] N. Zhao, T. P. Osedach, L.-Y. Chang, S. M. Geyer, D. Wanger, M. T. Binda, A. C. Arango, M. G. Bawendi, V. Bulovic, *ACS Nano* **2010**, *4*, 3743.
[25] K. J. Karki, J. R. Widom, J. Seibt, I. Moody, M. C. Lonergan, T. Pullerits, A. H. Marcus, *Nat. Commun.* **2014**, *5*, 5869.
[26] X. Yan, Y. Pei, H. Chen, J. Zhao, Z. Zhou, H. Wang, L. Zhang, J. Wang, X. Li, C. Qin, G. Wang, Z. Xiao, Q. Zhao, K. Wang, H. Li, D. Ren, Q. Liu, H. Zhou, J. Chen, P. Zhou, *Adv. Mater.* **2019**, *31*, 1805284.
[27] J. Guo, S. Guo, X. Su, S. Zhu, Y. Pang, W. Luo, J. Zhang, H. Sun, H. Li, D. Zhang, *ACS Appl. Electron. Mater.* **2020**, *2*, 827.
[28] Z. Wang, S. Joshi, S. E. Savel'ev, H. Jiang, R. Midya, P. Lin, M. Hu, N. Ge, J. P. Strachan, Z. Li, *Nat. Mater.* **2017**, *16*, 101.
[29] S. T. Han, L. Hu, X. Wang, Y. Zhou, Y. J. Zeng, S. Ruan, C. Pan, Z. Peng, *Adv. Sci.* **2017**, *4*, 1600435.
[30] Y. Wang, Z. Lv, J. Chen, Z. Wang, Y. Zhou, L. Zhou, X. Chen, S. T. Han, *Adv. Mater.* **2018**, *30*, 1802883.
[31] D. Parobek, Y. Dong, T. Qiao, D. H. Son, *Chem. Mater.* **2018**, *30*, 2939.
[32] A. Younis, D. Chu, X. Lin, J. Yi, F. Dang, S. Li, *ACS Appl. Mater. Interfaces* **2013**, *5*, 2249.
[33] I. Sanchez Esqueda, X. Yan, C. Rutherglen, A. Kane, T. Cain, P. Marsh, Q. Liu, K. Galatsis, H. Wang, C. Zhou, *ACS Nano* **2018**, *12*, 7352.
[34] X. Duan, Y. Huang, C. M. Lieber, *Nano Lett.* **2002**, *2*, 487.
[35] G. Milano, M. Luebben, Z. Ma, R. Dunin-Borkowski, L. Boarino, C. F. Pirri, R. Waser, C. Ricciardi, I. Valov, *Nat. Commun.* **2018**, *9*, 5151.
[36] W. Xu, S. Y. Min, H. Hwang, T. W. Lee, *Sci. Adv.* **2016**, *2*, e1501326.
[37] D. Liu, H. Li, L. Song, X. Zhu, Y. Qin, H. Zu, J. He, Z. Yang, F. Wang, *Nanotechnology* **2020**, *31*, 335202.
[38] X. Li, Y. Meng, R. Fan, S. Fan, C. Dang, X. Feng, J. C. Ho, Y. Lu, *Nano Res.* **2021**, https://doi.org/10.1007/s12274-021-3332-0.
[39] Y. Meng, C. Lan, F. Li, S. Yip, R. Wei, X. Kang, X. Bu, R. Dong, H. Zhang, J. C. Ho, *ACS Nano* **2019**, *13*, 6060.
[40] Y. Meng, Z. Lai, F. Li, W. Wang, S. Yip, Q. Quan, X. Bu, F. Wang, Y. Bao, T. Hosomi, *ACS Nano* **2020**, *14*, 12749.
[41] P. Feng, W. W. Xu, Y. Yang, X. Wan, Y. Shi, Q. Wan, J. W. Zhao, Z. Cui, *Adv. Funct. Mater.* **2017**, *27*, 1604447.
[42] P. H. Lau, K. Takei, C. Wang, Y. Ju, J. Kim, Z. Yu, T. Takahashi, G. Cho, A. Javey, *Nano Lett.* **2013**, *13*, 3864.
[43] M. Halter, L. Bégon-Lours, V. Bragaglia, M. Sousa, B. J. Offrein, S. Abel, M. Luisier, J. Fompeyrine, *ACS Appl. Mater. Interfaces* **2020**, *12*, 17725.
[44] S.-Y. Min, W.-J. Cho, *Sci. Rep.* **2020**, *10*, 15561.
[45] C. J. O'Kelly, J. A. Fairfield, D. McCloskey, H. G. Manning, J. F. Donegan, J. J. Boland, *Adv. Electron. Mater.* **2016**, *2*, 1500458.
[46] J. He, X. Liu, L. Song, H. Li, H. Zu, J. Li, H. Zhang, J. Zhang, Y. Qin, F. Wang, *J. Phys. Chem. Lett.* **2021**, *12*, 1339.
[47] Y. Meng, G. Liu, A. Liu, Z. Guo, W. Sun, F. Shan, *ACS Appl. Mater. Interfaces* **2017**, *9*, 10805.
[48] Y. Meng, K. Lou, R. Qi, Z. Guo, B. Shin, G. Liu, F. Shan, *ACS Appl. Mater. Interfaces* **2018**, *10*, 20703.
[49] Z. Zhou, C. Lan, R. Wei, J. C. Ho, *J. Mater. Chem. C* **2019**, *7*, 202.
[50] F. Li, S. Yip, R. Dong, Z. Zhou, C. Lan, X. Liang, D. Li, Y. Meng, X. Kang, J. C. Ho, *Nano Res.* **2019**, *12*, 1796.
[51] F. Li, Y. Meng, R. Dong, S. Yip, C. Lan, X. Kang, F. Wang, K. S. Chan, J. C. Ho, *ACS Nano* **2019**, *13*, 12042.
[52] L. A. Kong, J. Sun, C. Qian, Y. Fu, J. X. Wang, J. L. Yang, Y. L. Gao, *Org. Electron.* **2017**, *47*, 126.
[53] P. Gkoupidenis, D. A. Koutsouras, G. G. Malliaras, *Nat. Commun.* **2017**, *8*, 15448.
[54] Y. H. Liu, L. Q. Zhu, P. Feng, Y. Shi, Q. Wan, *Adv. Mater.* **2015**, *27*, 5599.
[55] R. Ge, X. Wu, M. Kim, J. Shi, S. Sonde, L. Tao, Y. Zhang, J. C. Lee, D. Akinwande, *Nano Lett.* **2018**, *18*, 434.
[56] R. Xu, H. Jang, M. H. Lee, D. Amanov, Y. Cho, H. Kim, S. Park, H. J. Shin, D. Ham, *Nano Lett.* **2019**, *19*, 2411.
[57] C. Pan, Y. Ji, N. Xiao, F. Hui, K. Tang, Y. Guo, X. Xie, F. M. Puglisi, L. Larcher, E. Miranda, L. Jiang, Y. Shi, I. Valov, P. C. McIntyre, R. Waser, M. Lanza, *Adv. Funct. Mater.* **2017**, *27*, 1604811.
[58] F.-S. Yang, M. Li, M.-P. Lee, I.-Y. Ho, J.-Y. Chen, H. Ling, Y. Li, J.-K. Chang, S.-H. Yang, Y.-M. Chang, *Nat. Commun.* **2020**, *11*, 2972.
[59] R. A. John, F. Liu, N. A. Chien, M. R. Kulkarni, C. Zhu, Q. Fu, A. Basu, Z. Liu, N. Mathews, *Adv. Mater.* **2018**, *30*, 1800220.
[60] H. Tian, Q. Guo, Y. Xie, H. Zhao, C. Li, J. J. Cha, F. Xia, H. Wang, *Adv. Mater.* **2016**, *28*, 4991.
[61] C. Lan, Z. Zhou, Z. Zhou, C. Li, L. Shu, L. Shen, D. Li, R. Dong, S. Yip, J. C. Ho, *Nano Res.* **2018**, *11*, 3371.
[62] C. Lan, D. Li, Z. Zhou, S. Yip, H. Zhang, L. Shu, R. Wei, R. Dong, J. C. Ho, *Small Methods* **2019**, *3*, 1800245.
[63] Y. Shi, X. Liang, B. Yuan, V. Chen, H. Li, F. Hui, Z. Yu, F. Yuan, E. Pop, H. S. P. Wong, M. Lanza, *Nat. Electron.* **2018**, *1*, 458.
[64] V. K. Sangwan, H.-S. Lee, H. Bergeron, I. Balla, M. E. Beck, K.-S. Chen, M. C. Hersam, *Nature* **2018**, *554*, 500.
[65] M. Kim, R. Ge, X. Wu, X. Lan, J. Tice, J. C. Lee, D. Akinwande, *Nat. Commun.* **2018**, *9*, 2524.
[66] M. Wang, S. Cai, C. Pan, C. Wang, X. Lian, Y. Zhuo, K. Xu, T. Cao, X. Pan, B. Wang, S.-J. Liang, J. J. Yang, P. Wang, F. Miao, *Nat. Electron.* **2018**, *1*, 130.
[67] H. Tian, W. Mi, X. F. Wang, H. Zhao, Q. Y. Xie, C. Li, Y. X. Li, Y. Yang, T. L. Ren, *Nano Lett.* **2015**, *15*, 8013.
[68] M. T. Sharbati, Y. Du, J. Torres, N. D. Ardolino, M. Yun, F. Xiong, *Adv. Mater.* **2018**, *30*, 1802353.
[69] L. Wang, Z. Wang, W. Zhao, B. Hu, L. Xie, M. Yi, H. Ling, C. Zhang, Y. Chen, J. Lin, J. Zhu, W. Huang, *Adv. Electron. Mater.* **2017**, *3*, 1600244.
[70] C. J. Wan, L. Q. Zhu, Y. H. Liu, P. Feng, Z. P. Liu, H. L. Cao, P. Xiao, Y. Shi, Q. Wan, *Adv. Mater.* **2016**, *28*, 3557.
[71] J. Zhu, Y. Yang, R. Jia, Z. Liang, W. Zhu, Z. U. Rehman, L. Bao, X. Zhang, Y. Cai, L. Song, R. Huang, *Adv. Mater.* **2018**, *30*, 1800195.
[72] H. Chen, X. Xue, C. Liu, J. Fang, Z. Wang, J. Wang, D. W. Zhang, W. Hu, P. Zhou, *Nat. Electron.* **2021**, *4*, 399.
[73] J. Jadwiszczak, D. Keane, P. Maguire, C. P. Cullen, Y. Zhou, H. Song, C. Downing, D. Fox, N. McEvoy, R. Zhu, J. Xu, G. S. Duesberg, Z. M. Liao, J. J. Boland, H. Zhang, *ACS Nano* **2019**, *13*, 14262.
[74] M. Yoshida, R. Suzuki, Y. Zhang, M. Nakano, Y. Iwasa, *Sci. Adv.* **2015**, *1*, e1500606.
[75] B. Standley, W. Bao, H. Zhang, J. Bruck, C. N. Lau, M. Bockrath, *Nano Lett.* **2008**, *8*, 3345.
[76] N. Lang, P. Avouris, *Phys. Rev. Lett.* **1998**, *81*, 3515.
[77] W. Li, X. Qian, J. Li, *Nat. Rev. Mater.* **2021**, https://doi.org/10.1038/s41578-021-00304-0.

[78] F. Zhang, H. Zhang, S. Krylyuk, C. A. Milligan, Y. Zhu, D. Y. Zemlyanov, L. A. Bendersky, B. P. Burton, A. V. Davydov, J. Appenzeller, *Nat. Mater.* **2019**, *18*, 55.
[79] X. Zhu, D. Li, X. Liang, W. D. Lu, *Nat. Mater.* **2019**, *18*, 141.
[80] L. Sun, Y. Zhang, G. Hwang, J. Jiang, D. Kim, Y. A. Eshete, R. Zhao, H. Yang, *Nano Lett.* **2018**, *18*, 3229.
[81] L. Sun, H. Yu, D. Wang, J. Jiang, D. Kim, H. Kim, S. Zheng, M. Zhao, Q. Ge, H. Yang, *2D Mater.* **2018**, *6*, 015029.
[82] J. Mannhart, D. G. Schlom, *Science* **2010**, *327*, 1607.
[83] R. Ramesh, D. G. Schlom, *Nat. Rev. Mater.* **2019**, *4*, 257.
[84] A. D. Caviglia, S. Gariglio, N. Reyren, D. Jaccard, T. Schneider, M. Gabay, S. Thiel, G. Hammerl, J. Mannhart, J. M. Triscone, *Nature* **2008**, *456*, 624.
[85] A. Tsukazaki, A. Ohtomo, T. Kita, Y. Ohno, H. Ohno, M. Kawasaki, *Science* **2007**, *315*, 1388.
[86] A. Tsukazaki, S. Akasaka, K. Nakahara, Y. Ohno, H. Ohno, D. Maryenko, A. Ohtomo, M. Kawasaki, *Nat. Mater.* **2010**, *9*, 889.
[87] P. Irvin, Y. Ma, D. F. Bogorin, C. Cen, C. W. Bark, C. M. Folkman, C.-B. Eom, J. Levy, *Nat. Photonics* **2010**, *4*, 849.
[88] D. Miron, D. Cohen-Azarzar, B. Hoffer, M. Baskin, S. Kvatinsky, E. Yalon, L. Kornblum, *Appl. Phys. Lett.* **2020**, *116*, 223503.
[89] H. Chen, Y. S. Rim, I. C. Wang, C. Li, B. Zhu, M. Sun, M. S. Goorsky, X. He, Y. Yang, *ACS Nano* **2017**, *11*, 4710.
[90] A. Tebano, E. Fabbri, D. Pergolesi, G. Balestrino, E. Traversa, *ACS Nano* **2012**, *6*, 1278.
[91] W. Meevasana, P. D. C. King, R. H. He, S. K. Mo, M. Hashimoto, A. Tamai, P. Songsiriritthigul, F. Baumberger, Z. X. Shen, *Nat. Mater.* **2011**, *10*, 114.
[92] C. Cen, S. Thiel, G. Hammerl, C. W. Schneider, K. Andersen, C. S. Hellberg, J. Mannhart, J. Levy, *Nat. Mater.* **2008**, *7*, 298.
[93] A. Rastogi, R. Budhani, *Opt. Lett.* **2012**, *37*, 317.
[94] J. Z. Li, J. Y. Lin, H. X. Jiang, M. Asif Khan, Q. Chen, *J. Appl. Phys.* **1997**, *82*, 1227.
[95] X. Dang, C. Wang, E. Yu, K. Boutros, J. Redwing, *Appl. Phys. Lett.* **1998**, *72*, 2745.
[96] M. L. Schneider, C. A. Donnelly, S. E. Russek, B. Baek, M. R. Pufall, P. F. Hopkins, P. D. Dresselhaus, S. P. Benz, W. H. Rippard, *Sci. Adv.* **2018**, *4*, e1701329.
[97] T. Paul, T. Ahmed, K. K. Tiwari, C. S. Thakur, A. Ghosh, *2D Mater.* **2019**, *6*, 045008.
[98] S. A. Siddiqui, S. Dutta, A. Tang, L. Liu, C. A. Ross, M. A. Baldo, *Nano Lett.* **2019**, *20*, 1033.
[99] S. Yang, J. Shin, T. Kim, K.-W. Moon, J. Kim, G. Jang, J. Yang, C. Hwang, Y. Jeong, J. P. Hong, *NPG Asia Mater.* **2021**, *13*, 11.
[100] P. Wang, M. E. Nasir, A. V. Krasavin, W. Dickson, A. V. Zayats, *Nano Lett.* **2020**, *20*, 1536.
[101] M.-K. Kim, J.-S. Lee, *Nano Lett.* **2019**, *19*, 2044.
[102] F. Tafuri, *Fundamentals and Frontiers of the Josephson Effect*, Springer Series in Materials Science, Vol. *286*, Springer International Publishing, Cham, Switzerland **2019**.
[103] M. L. Schneider, C. A. Donnelly, I. W. Haygood, A. Wynn, S. E. Russek, M. Castellanos-Beltran, P. D. Dresselhaus, P. F. Hopkins, M. R. Pufall, W. H. Rippard, *Sci. Rep.* **2020**, *10*, 934.
[104] U. S. Goteti, R. C. Dynes, *J. Appl. Phys.* **2021**, *129*, 073901.
[105] M. L. Schneider, C. A. Donnelly, S. E. Russek, *J. Appl. Phys.* **2018**, *124*, 161102.
[106] M.-J. Lee, D. H. Seo, S. M. Kwon, D. Kim, Y. Kim, W. S. Yun, J.-H. Cha, H.-K. Song, S. Lee, M. Jung, *ACS Nano* **2020**, *14*, 16114.
[107] X. Liu, D. Qu, H.-M. Li, I. Moon, F. Ahmed, C. Kim, M. Lee, Y. Choi, J. H. Cho, J. C. Hone, *ACS Nano* **2017**, *11*, 9143.
[108] S. Kim, D. H. Shin, C. O. Kim, S. S. Kang, J. M. Kim, C. W. Jang, S. S. Joo, J. S. Lee, J. H. Kim, S.-H. Choi, *ACS Nano* **2013**, *7*, 5168.
[109] L. Britnell, R. Gorbachev, R. Jalil, B. Belle, F. Schedin, A. Mishchenko, T. Georgiou, M. Katsnelson, L. Eaves, S. Morozov, *Science* **2012**, *335*, 947.
[110] C. Jia, M. Famili, M. Carlotti, Y. Liu, P. Wang, I. M. Grace, Z. Feng, Y. Wang, Z. Zhao, M. Ding, *Sci. Adv.* **2018**, *4*, eaat8237.
[111] S. G. Yi, M. U. Park, S. H. Kim, C. J. Lee, J. Kwon, G. H. Lee, K. H. Yoo, *ACS Appl. Mater. Interfaces* **2018**, *10*, 31480.
[112] C. Liu, X. Yan, X. Song, S. Ding, D. W. Zhang, P. Zhou, *Nat. Nanotechnol.* **2018**, *13*, 404.
[113] L. Liu, C. Liu, L. Jiang, J. Li, Y. Ding, S. Wang, Y.-G. Jiang, Y.-B. Sun, J. Wang, S. Chen, D. W. Zhang, P. Zhou, *Nat. Nanotechnol.* **2021**, *16*, 874.
[114] I. Žutić, J. Fabian, S. D. Sarma, *Rev. Mod. Phys.* **2004**, *76*, 323.
[115] T. Shibata, T. Shinohara, T. Ashida, M. Ohta, K. Ito, S. Yamada, Y. Terasaki, T. Sasaki, *Appl. Phys. Express* **2020**, *13*, 043004.
[116] K. M. Song, J.-S. Jeong, B. Pan, X. Zhang, J. Xia, S. Cha, T.-E. Park, K. Kim, S. Finizio, J. Raabe, *Nat. Electron.* **2020**, *3*, 148.
[117] E. Carlos, R. Branquinho, R. Martins, A. Kiazadeh, E. Fortunato, *Adv. Mater.* **2021**, *33*, 2004328.
[118] X. Zhang, S. Liu, X. Zhao, F. Wu, Q. Wu, W. Wang, R. Cao, Y. Fang, H. Lv, S. Long, *IEEE Electron Device Lett.* **2017**, *38*, 1208.
[119] P. Krzysteczko, J. Münchenberger, M. Schäfers, G. Reiss, A. Thomas, *Adv. Mater.* **2012**, *24*, 762.
[120] N. Locatelli, V. Cros, J. Grollier, *Nat. Mater.* **2014**, *13*, 11.
[121] D. Kim, H. Lu, S. Ryu, C.-W. Bark, C.-B. Eom, E. Tsymbal, A. Gruverman, *Nano Lett.* **2012**, *12*, 5697.
[122] M. L. Brongersma, N. J. Halas, P. Nordlander, *Nat. Nanotechnol.* **2015**, *10*, 25.
[123] J. Lambe, S. McCarthy, *Phys. Rev. Lett.* **1976**, *37*, 923.
[124] A. Emboras, A. Alabastri, P. Lehmann, K. Portner, C. Weilenmann, P. Ma, B. Cheng, M. Lewerenz, E. Passerini, U. Koch, *Appl. Phys. Lett.* **2020**, *117*, 230502.
[125] S. Song, J. Kim, S. M. Kwon, J. W. Jo, S. K. Park, Y. H. Kim, *Adv. Intell. Syst.* **2021**, *3*, 2000119.
[126] T. N. r. Török, M. Csontos, P. Makk, A. Halbritter, *Nano Lett.* **2020**, *20*, 1192.
[127] B. Sánta, Z. n. Balogh, L. s. Pósa, D. v. Krisztián, T. N. Török, D. n. Molnár, C. Sinkó, R. Hauert, M. Csontos, A. s. Halbritter, *ACS Appl. Mater. Interfaces* **2021**, *13*, 7453.
[128] M. Aono, T. Hasegawa, *Proc. IEEE* **2010**, *98*, 2228.
[129] J. J. Wagenaar, M. Morales-Masis, J. M. Van Ruitenbeek, *J. Appl. Phys.* **2012**, *111*, 014302.
[130] S. Oh, H. Hwang, I. Yoo, *APL Mater.* **2019**, *7*, 091109.
[131] S. Oh, T. Kim, M. Kwak, J. Song, J. Woo, S. Jeon, I. K. Yoo, H. Hwang, *IEEE Electron Device Lett.* **2017**, *38*, 732.
[132] H. Wang, Q. Zhao, Z. Ni, Q. Li, H. Liu, Y. Yang, L. Wang, Y. Ran, Y. Guo, W. Hu, *Adv. Mater.* **2018**, *30*, 1803961.
[133] B. Tian, L. Liu, M. Yan, J. Wang, Q. Zhao, N. Zhong, P. Xiang, L. Sun, H. Peng, H. Shen, *Adv. Electron. Mater.* **2019**, *5*, 1800600.
[134] E. Li, X. Wu, Q. Chen, S. Wu, L. He, R. Yu, Y. Hu, H. Chen, T. Guo, *Nano Energy* **2021**, *85*, 106010.
[135] S. Boyn, J. Grollier, G. Lecerf, B. Xu, N. Locatelli, S. Fusil, S. Girod, C. Carrétéro, K. Garcia, S. Xavier, *Nat. Commun.* **2017**, *8*, 14736.

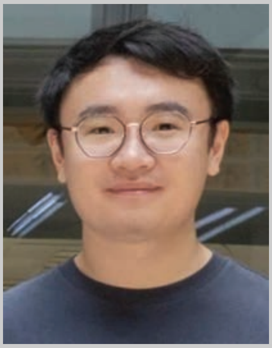

You Meng is a Ph.D. candidate in the Department of Materials Science and Engineering at the City University of Hong Kong. He received his B.S. and M.S. degree in Physics from the Qingdao University, China, in 2015 and 2018, respectively. His research interests mainly focus on nanomaterials-based neuromorphic electronics, photoconductive/photovoltaic photodetectors, field-effect/electrochemical transistors, etc.

Johnny C. Ho is a professor of Materials Science and Engineering at the City University of Hong Kong. He received his B.S. degree in Chemical Engineering, and his M.S. and Ph.D. degrees in Materials Science and Engineering from the University of California, Berkeley, in 2002, 2005, and 2009, respectively. From 2009 to 2010, he was a postdoctoral research fellow in the Nanoscale Synthesis and Characterization Group at Lawrence Livermore National Laboratory. His research interests focus on synthesis, characterization, integration, and device applications of nanoscale materials for various technological applications, including nanoelectronics, sensors, and energy harvesting.